# INFLUENCE OF BORON ON GAMMA-RAY SHIELDING EFFICIENCY OF CLAY MATERIAL

AKRAM M O H A M M E D D ALI

ISSN- 2394-5125 VOL 7, ISSUE 10, 2020

# INFLUENCE OF BORON ON GAMMA-RAY SHIELDING EFFICIENCY OF CLAY MATERIAL

**Akram Mohammed Ali [(1)] Ahmed Salih [(1)]**

[(1)] Physics Department, College of Science, University of Anbar
Corresponding author email: dr.akram@uoanbar.edu.iq

**Abstract**
In the present study, the gamma radiation shielding capability of clay as well as doped by boron was systematically investigated involving the measurement of linear attenuation coefficient and subsequently determination of shielding parameters at energy of 0.662 MeV for $^{137}$Cs. These include mass attenuation coefficient, mean free path, half layer value, tenth layer value, effective atomic number and electron density. In particular, it was noticeably found that increasing the prepared samples thickness leaded to higher values of mass attenuation coefficient (0.1065 cm$^2$ g$^{-1}$). Furthermore, samples treated with boron showed considerably higher mass attenuation coefficient values. In the free mean path, half layer values and tenth layer value profiles, the prepared materials showed an increased trend in conjunction with the thickness profile. The present work presents a new approach towards available, eco-friendly, cost-effective and efficient gamma radiation shielding materials.

**Keywords:** Clay, shielding, mass attenuation coefficient, boron

## 1. Introduction

The gamma radiation penetrating power is attributed to the established fact that gamma radiation possesses no mass or charge [1]. Therefore, shielding of gamma radiation can be efficiently implemented using materials that possess relatively high density and atomic mass number [2].

With the intention of reducing the ionizing radiation dose level to an acceptable limit, shielding in contradiction of high-energetic ionizing radiations is an absolute necessity [3]. Shielding materials with a certain nature and thickness are correlated to many factors such as the type of ionizing radiation, radio-isotope activity, exposure rate, and cost effectiveness [4-7]. Meanwhile, the exciting radiation shielding materials namely concrete and lead possess some major drawbacks such as high cost and toxicity. Remarkably, clay is considered a composite material that abundantly obtainable thus demonstrates a number of attractive properties such as non-poisonous, cost-effectiveness, and eco-friendly [1, 8]. These properties allow clay composites to be appropriate for shielding consideration [1, 2, 9-11].

I. Akkurt and H. Canakci (2011) demonstrated the investigation of linear attenuation coefficient using clay doped boron at different percentages. The corresponding outcomes augmented from 0.07 to 0.14 cm$^{-1}$ at 662 KeV with the increment of doped boron from 5% to 32% [12]. H.S. Mann, et al. studied the parameters of shielding effectiveness for light weight clay-fly ash bricks formed with different fly ash aggregates using $^{137}$Cs (661.6 keV), $^{241}$Am (59.4 keV), and $^{60}$Co (1173.2 keV and 1332.5 keV) sources [13]. They concluded that the utilized bricks are applicable to replace the commercial pure clay bricks whereby distance has no effect as a limitation. S. Olukotun et al. reported the capability of gamma radiation shielding for two types of clay-materials (Kaolin and Ball clay) [1]. In their study, the reported both experimental and theoretical mass attenuation coefficient ($\mu_s$) values. Whereby an upright agreement between the measured values and those obtained theoretically were obtained. In 2019, S. Tajudin et al., [14] evaluated the reflected and transmitted photons' spectrum and their ambient equivalent dose (Sv/photon) of specific material (clay) by Monte Carlo model.

Therefore, in this study, gamma radiation shielding capabilities of white clay-material are investigated by determining the theoretical and experimental values of the linear attenuation coefficient as well as the mass attenuation coefficient, $\mu/\rho$ (cm$^2$g$^{-1}$) of the clay materials using photon energy of 0.662 MeV emitted from cesium ($^{137}$Cs).

ISSN- 2394-5125 VOL 7, ISSUE 10, 2020

**2. Theory**

When a gamma-ray undergoes a certain sample thickness of x (cm), the photons are transmitted in accordance with the well-known Beer-Lambert's law [1].

$$I = I_o \exp(-\mu x) \quad (1)$$

Here, $I$ and $I_o$ are the intensity of gamma ray after and before passing via the thickness $t$ (cm), respectively. Whereby, $\mu$ ($cm^{-1}$) is the sample linear attenuation coefficient. Furthermore, the linear attenuation coefficient can also be presented in the means of $\mu_s$ ($cm^2\ g^{-1}$), which is illustrated in the following equation [1].

$$\mu = (\mu/\rho)\rho = \mu_s \quad (2)$$

Where ρ ($g\ cm^{-3}$) is the sample density. Herein, using Equation (2), Equation (1) is then written as follow:

$$I = I_o \exp(-\mu_s x) \quad (3)$$

In case a chemical compound or a mixture is used as an absorber, the is then calculated using Equation (4) [1].

$$\mu_s = \frac{\ln\left(\frac{I_o}{I}\right)}{\rho x} \quad (4)$$

The mean free path (MFP) is a crucial factor for determining the average distance between two interactions and it is measured in accordance with Equation (5) [1, 12].

$$MFP = \frac{1}{\mu(cm^{-1})} \quad (5)$$

The half-value layer (HVL), however, is an important parameter which is used to ascertain the material and/or mixture shielding capability. The HVL is evaluated in accordance with the following equation [12]:

$$HVL = \frac{ln2}{\mu} \quad (6)$$

Another crucial parameter is the tenth value layer (TVL) in which it represents the shielding material's thickness needed to lower the gamma radiation to its tenth intensity. The TVL can be estimated in accordance with Equation (7) [12].

$$TVL = \frac{ln10}{\mu} \quad (7)$$

The total photon interaction cross section ($\sigma_t$) of a material is evaluated with the assistance of ($\mu_s$) of that specific material through the following equation [15, 16]:

$$\sigma_t = M\mu_s/N_A \quad (8)$$

Where $N_A$ is denoted for the Avogadro's number and the value of $M$, which is the sample molecular weight, is calculated using the Equation (9)

$$M = \sum_i A_i n_i \quad (9)$$

herein $A_i$ is the earth element atomic number and $n_i$ is the molecule formula units number. The effective atomic cross section $\sigma_a$ is estimated using the subsequent equation, Equation (10) [15, 16]:

$$\sigma_a = \sigma_t / \sum_i n_i \quad (10)$$

Thus, the overall atomic cross-section is then determined with the help of Equation (11) [16].

$$\sigma_{t,a} = \mu_s M / N_A \sum_i n_i \quad (11)$$

The overall electronic cross-section is calculated by Equation (12) [15, 16]

$$\sigma_{t,el} = \frac{1}{N_A} \sum_i \frac{f_i}{Z_i} A_i (\mu_s)_i \quad (12)$$

ISSN- 2394-5125 VOL 7, ISSUE 10, 2020

where $f_i$ represents the element $i$ fractional abundance, while $Z_i$ denotes the constituent element atomic number [16].

The values of $Z_{eff}$ can then be calculated using Equation (13) and $N_E$ values is subsequently evaluated by employing Equation (14)

$$Z_{eff} = \sigma_{t,a}/\sigma_{t,e} \quad (13)$$

$$N_{eff} = Z_{eff}/A_{tot}(N_A n_{tot}) \quad (14)$$

here, $\sigma_{t,e}$ and $\sigma_{t,a}$ are the electronic and molecular cross sections, respectively. $A_{tot}$ is the total matter weight, while $n_{tot}$is the total number of atoms in matter [17].

**3. Undoped and boron doped clay preparation**

White clay was collected from, Al-Rutbah at the west of Al-Anbar governorate (33°N 40°E) in Iraq. The as-minded clay was crushed to suitable size and then dried at normal atmospheric conditions; in accordance to the American Society for Testing and Materials [18], the crushed sample was pulverized, sieved (mesh size of 2 μm) and then pelletized. Three set of samples were molded. The first set of samples were made of pure clay at room temperature (RT), while the second set of samples were also made of pure clay but baked using muffled furnace at temperature of 1000 °C for 1 hour. Finally, the third set were made of pure clay by doped with 2% of boron and later baked at 1000 °C for 1 hour. In addition, the three made sets were also varied in thickness whereby 0.5, 1 and 2 cm with diameter of 3 cm were made. Hereinafter, the prepared samples were denoted as W1, W2 and W3 (Figure 1) as for unbaked, baked white clay and baked doped clay with boron, respectively.

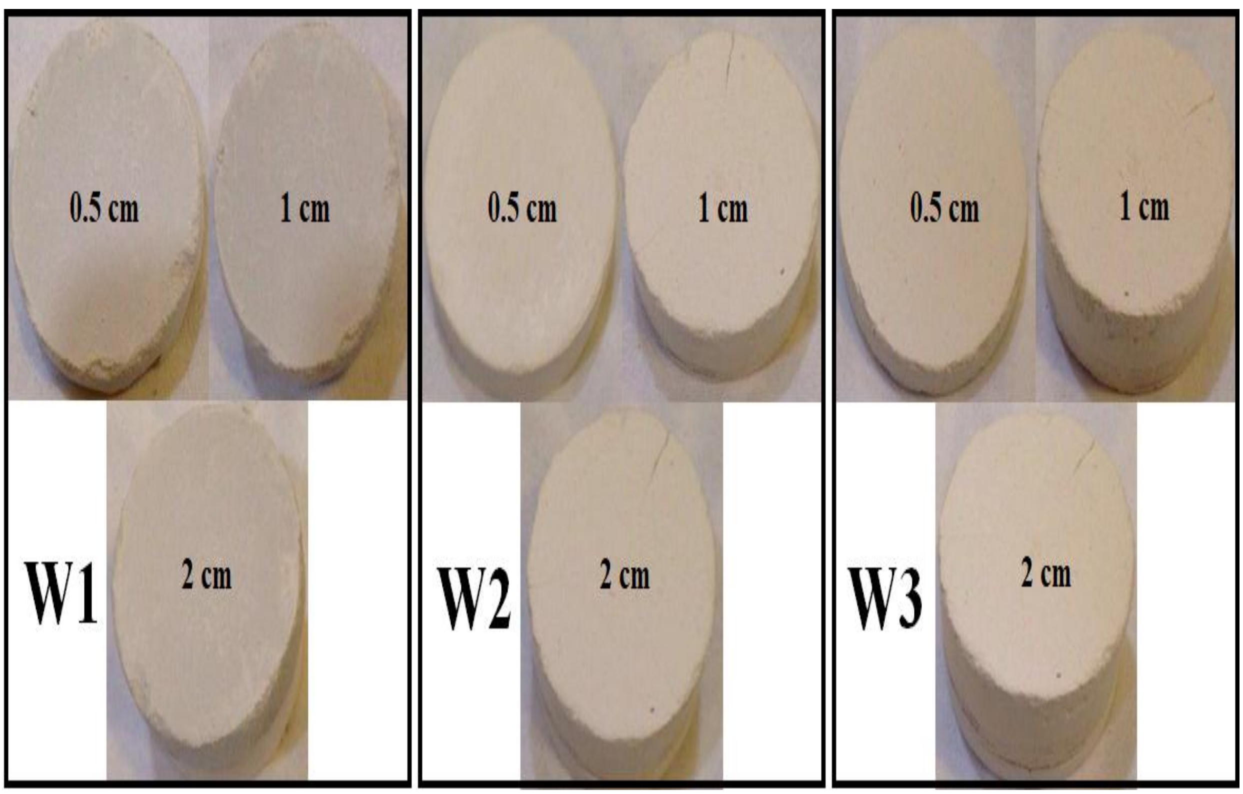


**Figure 1:** Samples preparation after compressed at different thicknesses and labelled W1, W2 and W3.

ISSN- 2394-5125 VOL 7, ISSUE 10, 2020

### 4. Results and discussion

In order to experimentally estimate the attenuation coefficient of the prepared samples, gamma-ray emission at 0.662 MeV emitted from $^{137}$Cs point source ($T_{1/2} = 30\ year$) was utilized in this study. As illustrated in Figure 2, the pelletized samples, at different thicknesses, backing temperatures and compositions, were placed between the NaI(TI) detector and the source. Subsequently, the data were recorded using Integrated Computer Spectrometer (PCI-ICS card) in conjunction with personal computer. The obtained data were utilized for the determination of the gamma radiation shielding capability parameters.

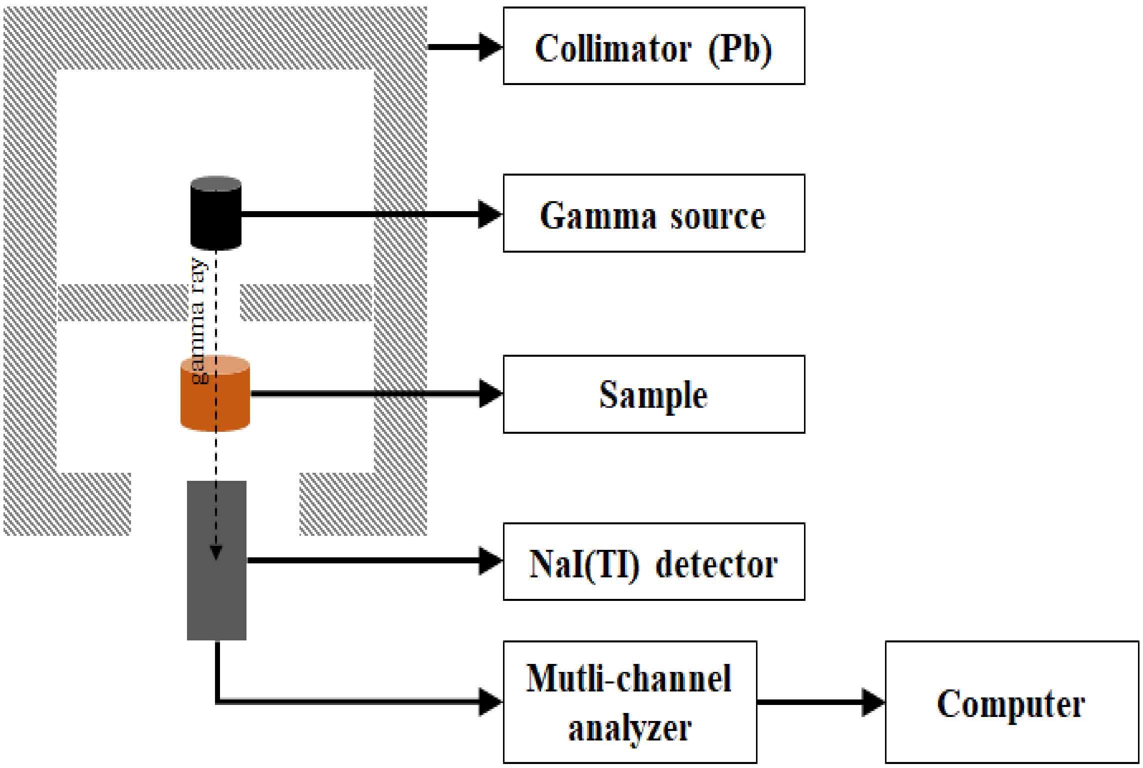


**Figure 2:** The measurement setup schematic illustration.

#### 4.1 Theoretical calculation by WinXCom

The shielding parameters (i.e. $\mu/\sigma$) required for the gamma radiation shielding capability of the pelletized samples were calculated using WinXCom software. The mentioned computer software can be utilized for the evaluation of total attenuation coefficient, photon scattering cross section, pair production and photoelectric absorption. While, Equation (15) and (16) were employed as the Bragg law.

$$\mu_s = \left(\frac{\mu}{\rho}\right)_{mix} = \sum_i \omega_i \left(\frac{\mu}{\rho}\right)_i \quad (15)$$

where $\omega_i$ is the fraction by weight of the element $i$ and given by:

$$\omega_i = \frac{a_i A_i}{\sum a_i A_i} \quad (16)$$

ISSN- 2394-5125 VOL 7, ISSUE 10, 2020

**Table 1:** Mass attenuation coefficient theoretical values of the compounds using WinXCom software at energy of 0.662 MeV.

| Compound | $\mu_s$ ($cm^2 g^{-1}$) | $\sigma_{t,a}$ (barn/atom) | $\sigma_{t,e}$ (barn/atom) | $Z_{eff}$ | $N_{el} x 10^{23}$ (electrons/g) |
|---|---|---|---|---|---|
| $SiO_2$ | 0.0773 | | 0.257 | | |
| $Si$ | 0.0361 | 2.570 | 0.040 | 10.000 | 3.01 |
| $O$ | 0.0412 | | 0.091 | | |
| $Al_2O_3$ | 0.0759 | | 0.257 | | |
| $Al$ | 0.0402 | 2.569 | 0.055 | 10.000 | 2.95 |
| $O$ | 0.0357 | | 0.071 | | |
| $Fe_2O_3$ | 0.0746 | | 0.260 | | |
| $Fe$ | 0.0522 | 3.956 | 0.074 | 15.200 | 2.87 |
| $O$ | 0.0224 | | 0.045 | | |
| $Na_2O$ | 0.0749 | | 0.256 | | |
| $Na$ | 0.0555 | 2.568 | 0.128 | 10.024 | 2.92 |
| $O$ | 0.0193 | | 0.021 | | |
| $K_2O$ | 0.0760 | | 0.258 | | |
| $K$ | 0.0631 | 3.962 | 0.144 | 15.333 | 2.94 |
| $O$ | 0.0129 | | 0.014 | | |
| $Ca_2CO_3$ | 0.0776 | | 0.258 | | |
| $Ca$ | 0.0444 | 3.010 | 0.049 | 11.667 | 3.01 |
| $C$ | 0.0066 | | 0.004 | | |
| $O$ | 0.0266 | | 0.044 | | |
| $MgO$ | 0.0768 | | 0.257 | | |
| $Mg$ | 0.0463 | 2.569 | 0.078 | 10.000 | 2.99 |
| $O$ | 0.0305 | | 0.051 | | |
| $TiO$ | 0.0733 | | 0.259 | | |
| $Ti$ | 0.0549 | 3.884 | 0.099 | 15.000 | 2.83 |
| $O$ | 0.0183 | | 0.030 | | |
| $B$ | 0.0714 | 1.280 | 0.256 | 5.000 | 2.79 |

Figure 3 demonstrates the theoretical values of the obtained ($\mu_s$) using WinXCom software at different energies ranging from 0.5 to 1.5 MeV for different compounds. As presented in Figure 3, the values of the ($\mu_s$) showed a decrease with the increment of the energy values. The mixtures used in the experimental work of this study were also investigated using WinXCom software.

The theoretical values such as linear attenuation coefficient, ($\mu_s$), $\sigma_{t,a}$, $\sigma_{t,el}$, $Z_{eff}$, and $N_{el}$ of clay and clay doped boron using WinXCom computer aided software are illustrated in Table 2. As shown in Table 2, these mixtures namely are $Al_2H_4O_9Si_2$ and $Al_2H_4O_9Si_2B_5$ for both clay and clay doped boron, respectively. It should be mentioned that the theoretical values presented in Table 2 are in a good agreement with the values obtained experimentally.

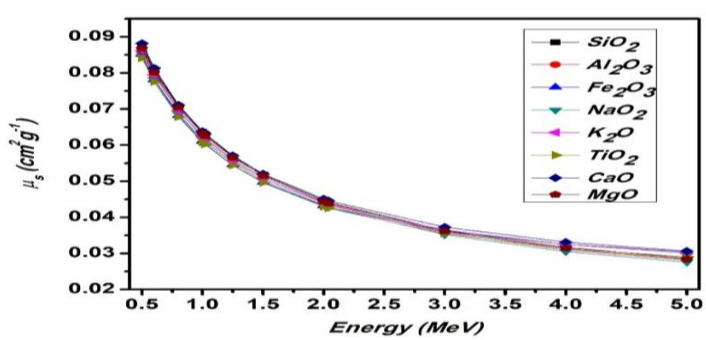


**Figure 3:** Mass attenuation coefficient values of different compounds.

ISSN- 2394-5125 VOL 7, ISSUE 10, 2020

**Table 2:** Theoretical values of both clay and clay doped boron with chemical formula $Al_2H_4O_9Si_2$ and $Al_2H_4O_9Si_2B_5$, respectively.

| Sample | $\mu_s$ $(cm^2 g^{-1})$ | $\sigma_{t,a}$ (barn/atom) | $\sigma_{t,e}$ (barn/atom) | $Z_{eff}$ | $N_{el} x 10^{23}$ (electrons/g) |
|---|---|---|---|---|---|
| ***Al₂H₄O₉Si₂*** | 0.0779 | 1.9646 | 0.2138 | 9.190 | 3.64 |
| *Al* | 0.0163 | | 0.0316 | | |
| *H* | 0.0012 | | 0.0307 | | |
| *O* | 0.0435 | | 0.1370 | | |
| *Si* | 0.0170 | | 0.0305 | | |
| **Sample** | $\mu_s$ $(cm^2 g^{-1})$ | $\sigma_{t,a}$ (barn/atom) | $\sigma_{t,e}$ (barn/atom) | $Z_{eff}$ | $N_{el} x 10^{23}$ (electrons/g) |
| ***Al₂H₄O₉Si₂B₅*** | 0.0768 | 1.8094 | 0.0709 | 25.519 | 1.08 |
| *Al* | 0.0133 | | 0.0241 | | |
| *H* | 0.0010 | | 0.0234 | | |
| *O* | 0.0354 | | 0.1043 | | |
| *Si* | 0.0138 | | 0.0233 | | |
| *B* | 0.0133 | | 0.0627 | | |

### 4.2 Attenuation coefficient, MFP, HVL, TVL $Z_{eff}$ and $N_{eff}$.

The obtained clays were found naturally with compositions itemized in Table 3.

**Table 3:** White clay chemical composition analysis by weight %.

| Materials composition | % | Mineralogy |
|---|---|---|
| $SiO_2$ | 48.1 | Kaolinite |
| $Al_2O_3$ | 34.7 | Illite |
| $Fe_2O_3$ | 1.07 | Smectite |
| $Na_2O$ | 0.29 | Quartz |
| $K_2O$ | 0.64 | Anatas |
| TiO | 1.23 | Halite |
| $Ca_2CO_3$ | 0.20 | |
| MgO | 0.39 | |
| Loss of ignition | 13.60 | |

Figure 4 illustrates a variation of the measured $\ln(\frac{I_o}{I})$ as a function of the prepared samples thickness. It can be clearly observed that the measured value increased with the prepared samples thickness increment. The correlation is generally utilized as an indicator of the linearity dependence.

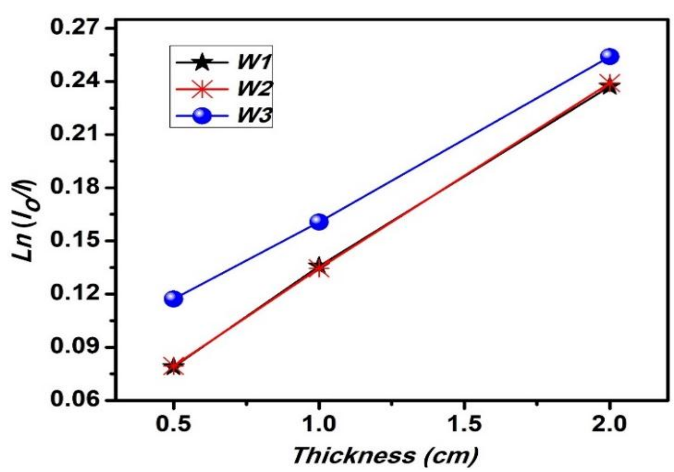


**Figure 4:** Variation of the measured $\ln(\frac{I_o}{I})$ with the prepared samples thickness.

Concurrently, the measured linear attenuation coefficient is elucidated in Figure 5 (a). A decrease in the values of the measured $(\mu)$ was noticed as the samples thickness increased from 0.5 to 2 cm. This can be mainly due to the relation between the $(\mu)$ and the $(x)$ is inversely proportional, in accordance with Equation (1). However, the values of the measured linear attenuation coefficient demonstrated an increment as the prepared unbaked samples were baked and further mixed with boron, as presented in Figure 5 (b).

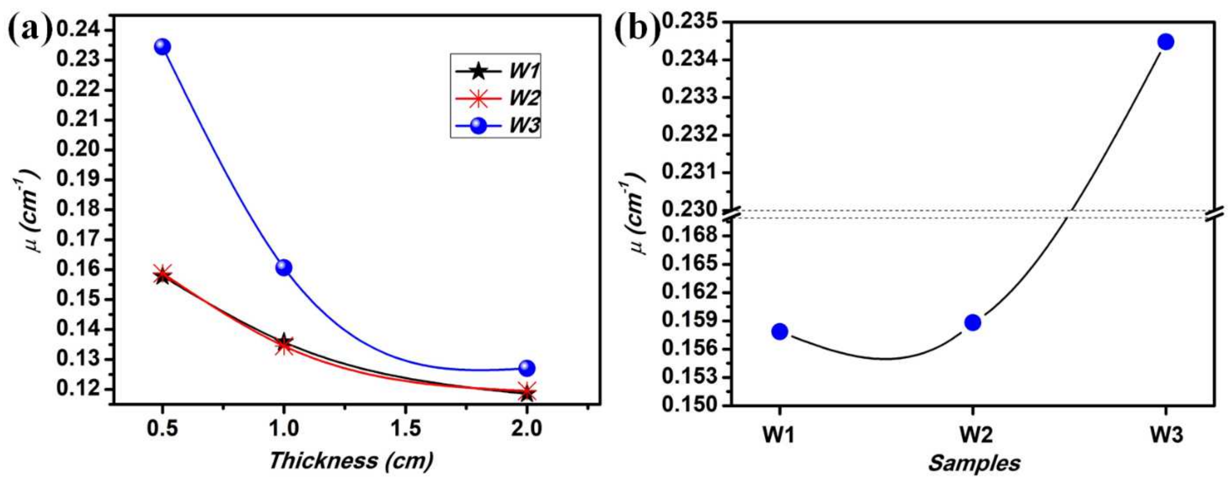


**Figure 5:** (a) variation of the linear attenuation coefficient with the prepared samples thickness and (b) samples taken at 0.5 cm in thickness for each sample as an indicator; section break was considered from 0.17 to 0.23 $cm^{-1}$.

Furthermore, the values of $(\mu_s)$, obtained using Equation 4, are demonstrated in Figure 6 where shown increasing the prepared samples thickness resulted in increased values of the calculated $(\mu_s)$. W3 sample (baked doped boron) showed different trend whereby a decrease in the $(\mu_s)$ values was observed as the thickness of the prepared sample was increased.

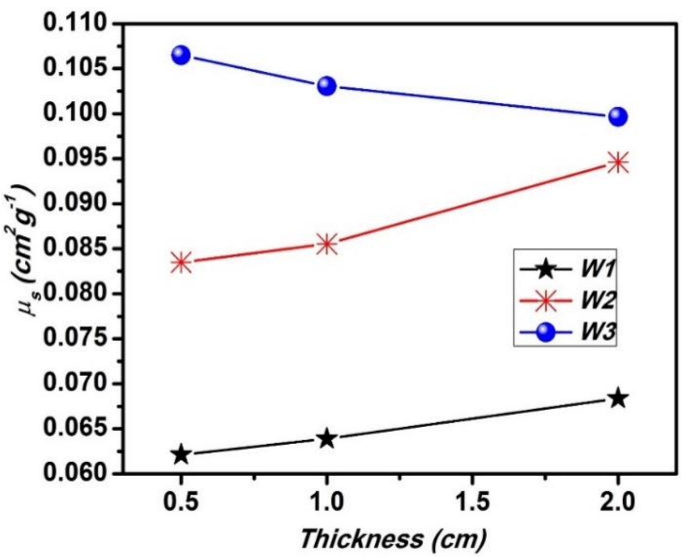


**Figure 6:** Variation of mass attenuation coefficient with the prepared materials thickness.

In the prospective of the prepared samples state of treatment (baked, unbaked, and baked doped boron), the $(\mu_s)$ increased linearly by means of process (Table 4). The values of $(\mu_s)$ were found to be 0.0621, 0.0835 and 0.1065 ($cm^2\,g^{-1}$) for 0.5 cm unbaked, baked, and baked doped boron, respectively. Moreover, the samples treated with boron showed higher values of the calculated $(\mu_s)$. This in turn can be mainly due to the effect of boron on the shielding capability of the utilized clay material [12, 19, 20]. These values were observed with higher $(\mu_s)$ profile as the thickness increased (Figure 6). In comparison with other results, our findings demonstrated higher ($\mu_s$) upon baking the sample [1]. Yet, baked doped boron samples showed considerably higher values of ($\mu_s$).

Consequently, Table 4 and Figure 7 show the calculated mean free path (MFP) which is calculated based on Equation (5) [15]. Regardless of the state of treatment, it can be obviously noticed from Table 4 that increase the prepared material thickness resulted in higher MFP values. Generally, the baked samples (W2) showed higher MFP values as compared to the unbaked samples (W1), with respect to the sample thickness. Adding boron to the mixture, however, decreased the values of MFP.

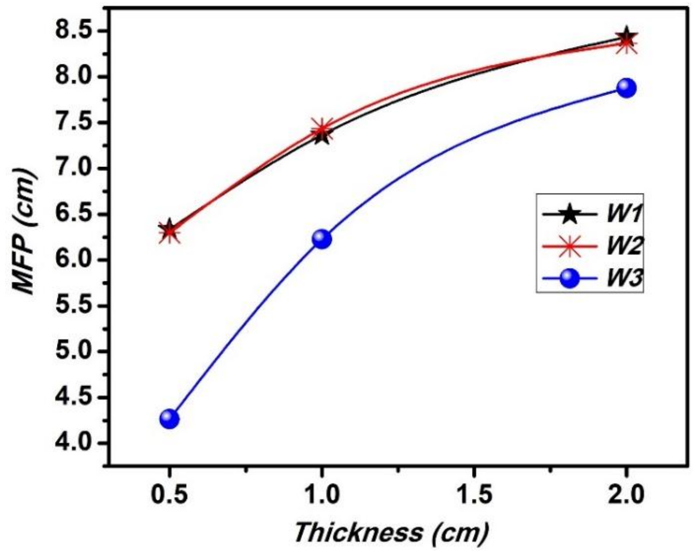


**Figure 7:** Mean free path of the prepared samples as a function of thickness.

Furthermore, both half value layer (HVL) and tenth value layer (TVL) are considered crucial parameters for the determination of shielding capability [16]. The related results of HVL and TVL are presented in Figure (8), Figure (9) and Table (4), respectively. From the profile of both HVL and TVL, it can be concluded that increasing the thickness of the prepared materials caused an increase in the mentioned parameters. However, adding boron to the clay-material leaded to a slight decrease in those parameters values. This indicates the usefulness of boron to be considered as an enhancement factor introduced to improve the shielding capability of clay-material.

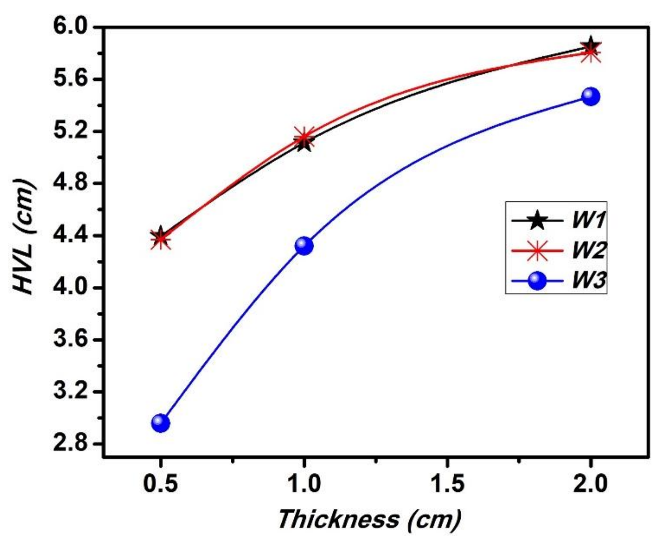


**Figure 8:** Half value layer of the prepared samples as a function of thickness.

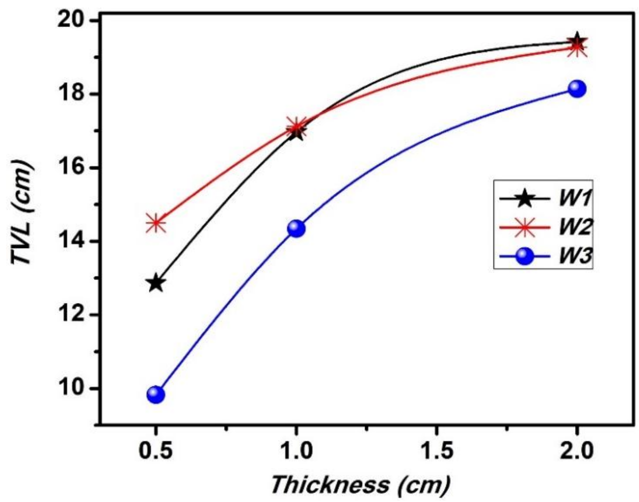


**Figure 9:** Tenth value layer of the prepared samples as a function of thickness.

The values of $Z_{eff}$ and $N_{el}$ in which the samples under test regarded results are presented in Table 4, respectively. It is worth mentioning that both values of $Z_{eff}$ and $N_{el}$ were calculated in accordance with Equations (13) and (14), respectively. It is clear to notice that samples W1 and W2 demonstrate the same values in regard to both $Z_{eff}$ and $N_{el}$. This can be mainly attributed to the fact that both $Z_{eff}$ and $N_{el}$ depend on the value of linear mass attenuation coefficient and ($\mu_s$) through Equations (8) through (14). It is also worth mentioning that the values of linear mass attenuation coefficient and ($\mu_s$) are nearly similar for the mentioned samples (W1 and W2). However, sample W3 (doped Boron) elucidated higher values of $Z_{eff}$ and $N_{el}$ due to the fact that the values of $Z_{eff}$ and $N_{el}$ are high as compared to W1 and W2 samples. A detailed illustration of the experimentally obtained ($\mu_s$), $\sigma_{t,a}$, $\sigma_{t,el}$, $Z_{eff}$, and $N_{el}$ for each compound (W1, W2, and W3) and its individual elements are tabulated in Table 5, Table 6 and Table 7, respectively.

**Table 4:** Experimental values of attenuation coefficient, MFP, HVL, TVL $Z_{eff}$ and $N_{el}$.

| Sample | Mass Attenuation Coefficients ($cm^2\ g^{-1}$) | | |
|---|---|---|---|
| | *W1* | *W2* | *W3* |
| 0.5 | 0.0621 | 0.0835 | 0.1065 |
| 1 | 0.0639 | 0.0856 | 0.1031 |
| 2 | 0.0684 | 0.0946 | 0.0997 |
| **Sample** | **Mean Free Path (cm)** | | |
| | *W1* | *W2* | *W3* |
| 0.5 | 6.335 | 6.296 | 4.265 |
| 1 | 7.367 | 7.435 | 6.227 |
| 2 | 8.433 | 8.367 | 7.876 |
| **Sample** | **Half Value Layer (cm)** | | |
| | *W1* | *W2* | *W3* |
| 0.5 | 4.397 | 4.370 | 2.960 |
| 1 | 5.113 | 5.160 | 4.321 |
| 2 | 5.853 | 5.806 | 5.466 |
| **Sample** | **Tenth Value Layer (cm)** | | |
| | *W1* | *W2* | *W3* |
| 0.5 | 14.587 | 14.498 | 9.820 |
| 1 | 16.963 | 17.119 | 14.337 |
| 2 | 19.418 | 19.265 | 18.136 |
| **Sample** | $Z_{eff}$ | | |
| | *W1* | *W2* | *W3* |

ISSN- 2394-5125 VOL 7, ISSUE 10, 2020

| | | | |
|---|---|---|---|
| 0.5 | 9.190 | 9.190 | 25.519 |
| 1 | 9.190 | 9.190 | 25.519 |
| 2 | 9.190 | 9.190 | 25.519 |
| **Sample** | $N_{el}$ | | |
| | ***W1*** | ***W2*** | ***W3*** |
| 0.5 | 3.644 | 3.644 | 10.825 |
| 1 | 3.644 | 3.644 | 10.825 |
| 2 | 3.644 | 3.644 | 10.825 |

Table 5: Experimentally attained ($\mu_s$), $\sigma_{t,a}$, $\sigma_{t,el}$, $Z_{eff}$, and $N_{el}$ for W1.

| ***Experimental at 0.662 MeV for ($Al_2H_4O_9Si_2$) unbacked (RT)*** | | | | | |
|---|---|---|---|---|---|
| ***compound/ element*** | $\mu_s$ ***($cm^2$/g)*** | $\sigma_{t,a}$ ***(barn/atom)*** | $\sigma_{t,el}$ ***(barn/atom)*** | $Z_{eff}$ | $N_e x10^{23}$ ***(electrons/g)*** |
| ***Thickness of 0.5 cm*** | | | | | |
| $Al_2H_4O_9Si_2$ | 0.0621 | 1.5670 | 0.1705 | 9.190 | 3.64 |
| *Al* | 0.0130 | | 0.0252 | | |
| *H* | 0.0010 | | 0.0245 | | |
| *O* | 0.0347 | | 0.1093 | | |
| *Si* | 0.0135 | | 0.0244 | | |
| ***Thickness of 1cm*** | | | | | |
| $Al_2H_4O_9Si_2$ | 0.0639 | 1.6111 | 0.1753 | 9.190 | 3.64 |
| *Al* | 0.0134 | | 0.0259 | | |
| *H* | 0.0010 | | 0.0252 | | |
| *O* | 0.0356 | | 0.1123 | | |
| *Si* | 0.0139 | | 0.0250 | | |
| ***Thickness of 2cm*** | | | | | |
| $Al_2H_4O_9Si_2$ | 0.0684 | 1.7245 | 0.1877 | 9.190 | 3.64 |
| *Al* | 0.0143 | | 0.0277 | | |
| *H* | 0.0011 | | 0.0269 | | |
| *O* | 0.0381 | | 0.1202 | | |
| *Si* | 0.0149 | | 0.0268 | | |

Table 6: Experimentally attained ($\mu_s$), $\sigma_{t,a}$, $\sigma_{t,el}$, $Z_{eff}$, and $N_{el}$ for W2.

| ***Experimental at 0.662 MeV for white clay ($Al_2H_4O_9Si_2$) baked (1000 °C)*** | | | | | |
|---|---|---|---|---|---|
| ***compound/ element*** | $\mu_s$ ***($cm^2$/g)*** | $\sigma_{t,a}$ ***(barn/atom)*** | $\sigma_{t,el}$ ***(barn/atom)*** | $Z_{eff}$ | $N_e x10^{23}$ ***(electrons/g)*** |
| ***Thickness of 0.5cm*** | | | | | |
| $Al_2H_4O_9Si_2$ | 0.0835 | 2.1052 | 0.2291 | 9.190 | 3.64 |
| *Al* | 0.0175 | | 0.0339 | | |
| *H* | 0.0013 | | 0.0329 | | |
| *O* | 0.0466 | | 0.1468 | | |
| *Si* | 0.0182 | | 0.0327 | | |
| ***Thickness of 1cm*** | | | | | |
| $Al_2H_4O_9Si_2$ | 0.0856 | 2.1573 | 0.2347 | 9.190 | 3.64 |
| *Al* | 0.0179 | | 0.0347 | | |
| *H* | 0.0013 | | 0.0337 | | |
| *O* | 0.0477 | | 0.1504 | | |
| *Si* | 0.0186 | | 0.0335 | | |
| ***Thickness of 2cm*** | | | | | |
| $Al_2H_4O_9Si_2$ | 0.0946 | 2.3858 | 0.2596 | 9.190 | 3.64 |

| | | | | | |
|---|---|---|---|---|---|
| *Al* | 0.0198 | | 0.0384 | | |
| *H* | 0.0015 | | 0.0373 | | |
| *O* | 0.0528 | | 0.1663 | | |
| *Si* | 0.0206 | | 0.0371 | | |

Table 7: Experimentally attained ($\mu_s$), $\sigma_{t,a}$, $\sigma_{t,el}$, $Z_{eff}$, and $N_{el}$ for W2.

| ***Xcom at 0.662 MeV for white clay + Baron ($Al_2H_4O_9Si_2B_5$)*** | | | | | |
|---|---|---|---|---|---|
| ***compound/ element*** | ***$\mu_s$ ($cm^2/g$)*** | ***$\sigma_{t,a}$ (barn/atom)*** | ***$\sigma_{t,el}$ (barn/atom)*** | ***$Z_{eff}$*** | ***$N_e x10^{23}$ (electrons/g)*** |
| ***Thickness of 0.5 cm*** | | | | | |
| ***$Al_2H_4O_9Si_2B_5$*** | 0.1065 | 2.5099 | 0.0984 | 25.519 | 10.8 |
| ***Al*** | 0.0184 | | 0.0334 | | |
| ***H*** | 0.0014 | | 0.0324 | | |
| ***O*** | 0.0491 | | 0.1447 | | |
| ***Si*** | 0.0192 | | 0.0323 | | |
| ***B*** | 0.0184 | | 0.0869 | | |
| ***Thickness of 1 cm*** | | | | | |
| ***$Al_2H_4O_9Si_2B_5$*** | 0.1031 | 2.4291 | 0.0952 | 25.519 | 10.8 |
| ***Al*** | 0.0178 | | 0.0323 | | |
| ***H*** | 0.0013 | | 0.0314 | | |
| ***O*** | 0.0475 | | 0.1400 | | |
| ***Si*** | 0.0185 | | 0.0312 | | |
| ***B*** | 0.0178 | | 0.0841 | | |
| ***Thickness of 2 cm*** | | | | | |
| ***$Al_2H_4O_9Si_2B_5$*** | 0.0997 | 2.3487 | 0.0920 | 25.519 | 10.8 |
| ***Al*** | 0.0172 | | 0.0312 | | |
| ***H*** | 0.0013 | | 0.0303 | | |
| ***O*** | 0.0460 | | 0.1354 | | |
| ***Si*** | 0.0179 | | 0.0302 | | |
| ***B*** | 0.0173 | | 0.0813 | | |

## Conclusion

White clay material as gamma radiation shielding was examined as raw material and as boron doped with different thicknesses to enhance the shielding capability. The ($\mu_s$) was calculated at 0.62 MeV radiation energy. Accordingly, the results indicate higher shielding capability as compared with previous reported data (0.1065 $cm^2$ $g^{-1}$). Furthermore, the MFP, HVL, and TVL were estimated theoretically gives results demonstrated higher values in conjunction with boron doped to the utilized material. The demonstrated work offers a new available and cost-effective alternative to the expensive concrete.

## Acknowledgement

The authors would like to offer great deal of appreciations to the Ministry of Higher Education and Scientific Research-Iraq as well as the University of Anbar for supporting this research.

## Conflict of interest

The authors declare no conflict of interest.

## References

[1] S. Olukotun, S. Gbenu, F. Ibitoye, O. Oladejo, H. Shittu, M. Fasasi, F. Balogun, Investigation of gamma radiation shielding capability of two clay materials, Nuclear Engineering and Technology, 50 (2018) 957-962.
[2] N. Alallak, S. Sarhan, Factors affecting gamma ray transmission, (2012).
[3] S. Kaur, A. Kaur, P.S. Singh, T. Singh, Scope of Pb-Sn binary alloys as gamma rays shielding material, Progress in Nuclear Energy, 93 (2016) 277-286.

ISSN- 2394-5125 VOL 7, ISSUE 10, 2020

[4] O. Agar, M. Sayyed, F. Akman, H. Tekin, M. Kaçal, An extensive investigation on gamma ray shielding features of Pd/Ag-based alloys, Nuclear Engineering and Technology, 51 (2019) 853-859.
[5] M.A. Jawad, M.A. Elwi, E.Y. Salih, T.A. Elwi, Z. Abbas, Monitoring the dielectric properties and propagation conditions of mortar for modern wireless mobile networks, Progress In Electromagnetics Research, 89 (2020) 91-97.
[6] A. Morioka, S. Sato, M. Kinno, A. Sakasai, J. Hori, K. Ochiai, M. Yamauchi, T. Nishitani, A. Kaminaga, K. Masaki, Irradiation and penetration tests of boron-doped low activation concrete using 2.45 and 14 MeV neutron sources, Journal of nuclear materials, 329 (2004) 1619-1623.
[7] Y. Abdullah, Cement-boron carbide concrete as radiation shielding material, Journal of Nuclear and related technologies, 7 (2010) 74-79.
[8] J.A. Omotoyinbo, O. Oluwole, Working properties of some selected refractory clay deposits in South Western Nigeria, (2008).
[9] B.L. Cohen, Concepts of nuclear physics, Tata McGraw-Hill Education, 1971.
[10] E. Blizard, J. Miller, Radiation attenuation characteristics of structural concrete, in, Oak Ridge National Lab., Tenn., 1958.
[11] E. Yılmaz, H. Baltas, E. Kırıs, I. Ustabas, U. Cevik, A. El-Khayatt, Gamma ray and neutron shielding properties of some concrete materials, Annals of Nuclear Energy, 38 (2011) 2204-2212.
[12] I. Akkurt, H. Canakci, Radiation attenuation of boron doped clay for 662, 1173 and 1332 keV gamma rays, (2011).
[13] H.S. Mann, G. Brar, G. Mudahar, Gamma-ray shielding effectiveness of novel light-weight clay-flyash bricks, Radiation Physics and Chemistry, 127 (2016) 97-101.
[14] S. Tajudin, A. Sabri, M.A. Aziz, S. Olukotun, B. Ojo, M. Fasasi, Feasibility of clay-shielding material for low-energy photons (Gamma/X), Nuclear Engineering and Technology, 51 (2019) 1633-1637.
[15] S.A. Issa, M. Sayyed, M. Zaid, K. Matori, Photon parameters for gamma-rays sensing properties of some oxide of lanthanides, Results in Physics, 9 (2018) 206-210.
[16] S.A. Issa, Effective atomic number and mass attenuation coefficient of PbO–BaO–B2O3 glass system, Radiation Physics and Chemistry, 120 (2016) 33-37.
[17] F. Akman, V. Turan, M. Sayyed, F. Akdemir, M. Kaçal, R. Durak, M. Zaid, Comprehensive study on evaluation of shielding parameters of selected soils by gamma and X-rays transmission in the range 13.94–88.04 keV using WinXCom and FFAST programs, Results in Physics, 15 (2019) 102751.
[18] J.M. Akande, S.A. Agbalajobi, Analysis on some physical and chemical properties of Oreke dolomite deposit, (2013).
[19] O. Içelli, K.S. Mann, Z. Yalçın, S. Orak, V. Karakaya, Investigation of shielding properties of some boron compounds, Annals of Nuclear Energy, 55 (2013) 341-350.
[20] E. Zorla, C. Ipbüker, A. Biland, M. Kiisk, S. Kovaljov, A.H. Tkaczyk, V. Gulik, Radiation shielding properties of high performance concrete reinforced with basalt fibers infused with natural and enriched boron, Nuclear engineering and Design, 313 (2017) 306-318.